

To appear in The Astrophysical Journal

The Velocity Function of Galaxies

Anthony H. Gonzalez and Kurtis A. Williams
 Department of Astronomy and Astrophysics
 University of California at Santa Cruz
 Santa Cruz, CA 95064

James S. Bullock, Tsafir S. Kolatt, and Joel R. Primack
 Department of Physics
 University of California at Santa Cruz
 Santa Cruz, CA 95064

ABSTRACT

We present a galaxy circular velocity function, $\Psi(\log v)$, derived from existing luminosity functions and luminosity-velocity relations. Such a velocity function is desirable for several reasons. First, it enables an objective comparison of luminosity functions obtained in different bands and for different galaxy morphologies, with a statistical correction for dust extinction. In addition, the velocity function simplifies comparison of observations with predictions from high-resolution cosmological N-body simulations.

We derive velocity functions from five different data sets and find rough agreement among them, but about a factor of 2 variation in amplitude. These velocity functions are then compared with N-body simulations of a Λ CDM model (corrected for baryonic infall) in order to demonstrate both the utility and current limitations of this approach. The number density of dark matter halos and the slope of the velocity function near v_* , the circular velocity corresponding to an $\sim L_*$ spiral galaxy, are found to be comparable to that of observed galaxies. The primary sources of uncertainty in construction of $\Psi(\log v)$ from observations and N-body simulations are discussed and explanations are suggested to account for these discrepancies.

Subject headings: galaxies: luminosity function, mass function, halos – cosmology:theory – dark matter

1. Introduction

Galaxy luminosity functions and the Tully-Fisher (TF) relation are key tools for testing models of galaxy formation and incorporating them into a larger picture of gravitational structure formation. An ultimate goal is to be able to reproduce these quantities starting from cosmological N-body

simulations. A significant complication is that observed galaxy luminosities are dependent upon a number of astrophysical processes (e.g., star formation history, gas cooling, internal extinction, supernovae feedback, chemical evolution, gas reheating and sharing between galaxies, stellar mass functions, etc.). These factors, which are generally poorly constrained, obscure the connection between formation processes and observable quantities.

These complications have not however deterred attempts to bridge the gap between the dark matter halos generated by N-body simulations and observed galaxies. In the past decade, the use of semi-analytic models (SAMs), which create galaxies from dark matter halos by modelling the relevant baryonic physics as global galaxy properties, has become the favored technique for tackling this issue. SAMs have had impressive success in reproducing both observed luminosity functions and TF relations, although not always both at the same time (Kauffmann, White, & Guiderdoni 1993, Cole et al. 1994, Somerville & Primack 1999). A limitation of this approach is that the current models necessarily contain many degrees of freedom, and a number of aspects of the models are oversimplified (Somerville & Primack 1999).

An alternative approach that complements the SAMs is the use of observational data to generate quantities that may be linked more directly with dissipationless N-body simulations. One such quantity is the galaxy velocity function, $\Psi(\log v_c)$, which describes the number density of galaxies per unit circular velocity. $\Psi(\log v_c)$ can be constructed using published luminosity functions and luminosity-velocity ($l-v$) relations. The velocity function is valuable for several reasons. First, conversion of luminosity functions into velocity functions places surveys obtained in different bands on equal footing (with the caveats discussed in §4.2). This permits direct comparison of the surveys and provides a single target function for which the simulations can aim. Second, by removing the need to model luminosity or understand the physical origin of the TF relation, a number of processes modelled by standard SAMs can be ignored. Only processes that affect baryonic infall, and hence the gravitational potential, impact the velocity function (see §4.3). These include gas cooling and supernovae feedback. For these reasons, the velocity function can be a useful tool for probing the connection between large scale gravitational physics and galaxy formation when coupled with the latest generation of cosmological N-body simulations.

Construction of a velocity function was suggested by Cole and Kaiser (1989), and an empirical velocity function was created by Shimasaku (1993). The latter work utilized a sample of nearby, bright galaxies from the *Third Reference Catalogue of Bright Galaxies* (de Vaucouleurs et al. 1991), with velocities derived from a combination of 21 cm observations and $l-v$ relations. Interestingly, Shimasaku also extended this analysis to attempt to include clusters, finding that the galaxy and cluster velocity functions are consistent with being derived from a single dynamical population.

The goal of this paper is to determine $\Psi(\log v_c)$. The approach taken will be first to use the luminosity function from a single survey (SSRS2) and a single set of $l-v$ relations to create a detailed velocity function. This analysis will be used to assess the importance of correctly accounting for factors that may alter the resultant $\Psi(\log v_c)$, such as internal galactic extinction. The results will

then be used as a foundation for production of simplified velocity functions for a variety of surveys and $l-v$ relations to assess the robustness of the results. It will be demonstrated that the derived velocity function is robust to within a factor of 2 for $70 \lesssim v_c \lesssim 260 \text{ km s}^{-1}$. To illustrate this we use the results from Adaptive Refinement Tree simulations (ART, Kravtsov, Klypin, & Khokhlov 1997, Klypin et al. 1999b). Comparison with these results shows agreement between observations and theory at $v \sim v_*$, but an excess of dark matter halos at lower velocities.

With the goal of fostering improvement beyond the current work, we also attempt to identify here the primary observational and theoretical sources of uncertainty. Among the observational limitations, uncertainties associated with the spiral and elliptical $l-v$ relations prove to be the most significant factors. Among the theoretical issues, correction of dissipationless models for the uncertain effects of baryonic infall is one of the most significant sources of uncertainty.

In §2 we define the velocity function. The various ingredients necessary to construct this function are detailed in §3. Then we turn to the data analysis in §4, where we also compare the derived velocity functions with the N-body simulation and discuss sources of uncertainty. We discuss our results and conclusions in §5. Throughout this paper the Hubble parameter is expressed as $H_0 = 100 h \text{ km s}^{-1} \text{ Mpc}^{-1}$.

2. Schechter Velocity Functions

Galaxy luminosity functions are normally parameterized using a Schechter function (Schechter 1976) of the form

$$\Phi(L)dL = \Phi_* \left(\frac{L}{L_*}\right)^\alpha \exp\left(-\frac{L}{L_*}\right) \frac{dL}{L_*}, \quad (1)$$

where the three observationally determined parameters Φ_* , α , and L_* respectively describe the normalization, faint end slope, and break point of the luminosity function. If the velocity, v , is related to L by a simple power law ($L = Av^n$), the number density of galaxies per unit velocity can also be described by a generalized form of the Schechter function,

$$\tilde{\Psi}(v)dv = \tilde{\Psi}_* \left(\frac{v}{v_*}\right)^\beta \exp\left[-\left(\frac{v}{v_*}\right)^n\right] \frac{dv}{v_*}, \quad (2)$$

where $v_* = (L_*/A)^{1/n}$, $\beta \equiv n(\alpha + 1) - 1$, and $\tilde{\Psi}_* \equiv n\Phi_*$ (see Appendix). Equivalently, this can be expressed in terms of $\eta = \log(v)$ as,

$$\Psi(\eta)d\eta = \Psi_* (10^{\eta-\eta_*})^{\beta+1} \exp\left[-(10^{\eta-\eta_*})^n\right] d\eta, \quad (3)$$

where $\Psi_* = (\ln 10)\tilde{\Psi}_*$. Luminosity-velocity relations exhibit tight correlation, so we choose to construct a circular velocity function for comparison with cosmological models. Specifically, we

define v_c to be the circular velocity measured in the flat part of a spiral galaxy’s rotation curve. For spirals v_c can be observed directly; for ellipticals the velocity dispersion, σ , is observed, and so it is necessary to convert σ to v_c . In this paper, the simplifying assumption is made that an elliptical can be modeled as an isothermal sphere, in which case $v_c = \sqrt{2}\sigma$ (Binney & Tremaine 1987). The quantity v_c can also be extracted from very high-resolution N-body simulations, so a direct comparison of observed and simulated $\Psi(\log v_c)$ is possible.

3. Velocity Function Ingredients

3.1. Survey Luminosity Functions

We impose several criteria on the input luminosity function to simplify the analysis. First, it is preferable that the selected survey contain a large number of galaxies, encompass a large volume, and extend to luminosities well below L_* . Second, morphological information is necessary since spirals, ellipticals, and irregulars are observed to follow different $l - v$ relations. Table 1 lists a number of recent surveys for which luminosity functions have been computed, as well as Schechter parameters and the approximate magnitude range over which the Schechter fit is valid. Only the CfA2, SSRS2, and APM surveys meet the above criteria (Marzke et al. 1994, Marzke et al. 1998). The APM luminosity functions derived for different morphological types have been called into question by several groups however (Marzke et al. 1994, Zucca, Pozzetti, & Zamorani 1994), and so we refrain from using this morphological data. Also, although it lacks morphological information, the Las Campanas Redshift Survey (LCRS) spectroscopically subdivides the galaxy population in a manner that roughly corresponds to morphological types (Bromley et al. 1998).

There are other practical considerations regarding the $l - v$ relations that impose further constraints on which surveys can be utilized. In particular, the CfA survey uses the Zwicky magnitude system, for which $l - v$ relations are not published for any morphological type. The situation is slightly better for the R -band LCRS; the R -band Tully-Fisher relation is well-studied and exhibits a tight correlation, but similar information is not available for ellipticals or irregulars. In fact, $l - v$ relations have thus far been published for all morphological types only in the B -band. Consequently, for our initial effort at generating $\Psi(\log v_c)$ we select the B -band SSRS2 survey. We use the Schechter luminosity function parameters derived for the SSRS2 survey assuming no Virgocentric infall, and note that Virgocentric infall corrections to the luminosity function have only a modest effect on the results (Marzke et al. 1998).

3.2. Luminosity-Velocity relations

The observational limitations of luminosity-velocity relations pose the greatest challenge to construction of the velocity function. Derivation of $\Psi(\log v_c)$ requires that well-calibrated $l - v$

relations exist for all morphological types that contribute significantly to the luminosity function.

For spirals the forward Tully-Fisher (TF) relation ($M = a - b[\log 2v_c - 2.5]$) has been extensively studied (Tully & Fisher 1977). Independent analyses have generated consistent results in the I - and R -bands and have demonstrated that the intrinsic scatter in the relation is $\lesssim 0.4$ mag at these wavelengths (Willick et al. 1996). In the B -band less effort has been expended towards calibration of the TF relation because the observed scatter is greater than at longer wavelengths. Still, several calibrations have been published. In particular, the TF relation derived in the work of Yasuda, Fukugita, and Okamura (1997) is chosen for construction of the SSRS2 velocity function. Table 2 lists TF parameters derived by various authors in B , R , and K . The different B -band relations will be used to evaluate the effect of the choice of TF parameters on the derived $\Psi(\log v_c)$. Also given in Table 2 is the velocity range spanned by the data used to define each relation. It is important to note that in no case has the TF relation been defined above ~ 350 km s $^{-1}$. Data is also sparse below ~ 100 km s $^{-1}$, but the work that has been done for both spirals and dwarfs at lower circular velocities indicates that there is no dramatic departure from the TF relation down to $v_c \lesssim 20$ km s $^{-1}$ (Hoffman et al. 1996, Richter, Tammann, & Huchtmeier 1987).

For ellipticals the D_n - σ relation is the most accurate means of converting luminosity to velocity dispersion (Dressler et al. 1987). However, SSRS2 and other existing large surveys do not publish effective radii and luminosities for individual galaxies. Since the SSRS2 gives only a luminosity function for the E/S0 population, the Faber-Jackson (FJ, Faber & Jackson 1976) relation must be employed. Unfortunately, subsequent to the development of the D_n - σ relation scant effort has been given to calibration of the FJ relation, and so we refer to early work by de Vaucouleurs & Olson 1982. Using a sample of 86 E's and S0's with recessional velocities greater than 1550 km s $^{-1}$ and $135 < \sigma < 376$ km s $^{-1}$, these authors observe that

$$L_{B_T} \propto \sigma^{3.08 \pm 0.28}, \quad (4)$$

or

$$M_{B_T} = (-19.71 \pm 0.08) + (7.7 \pm 0.7) (\log \sigma - 2.3) + 5 \log h. \quad \text{“Best”} \quad (5)$$

Although this is the relation used for the SSRS2 analysis, we caution that the statistical error may be a significant underestimate of the uncertainty in this relation. A larger sample of pure E's in the same paper yields

$$M_{B_T} = (-19.38 \pm 0.08) + (9.0 \pm 0.7) (\log \sigma - 2.3) + 5 \log h. \quad \text{“High”} \quad (6)$$

For the remainder of the paper these will respectively be denoted as the “Best” and “High” FJ relations, as they represent our best estimate of the true relation and the relation with the highest probable slope. The error associated with the slope of the FJ relation has a negligible effect on the results, but the difference in zeropoints is a significant source of uncertainty.

For irregulars, the $l - v$ relationship remains poorly constrained. Fortunately, this does not impede the calculation of $\Psi(\log v_c)$ because irregulars are only a trace population in the velocity regime ($v_c \gtrsim 100 \text{ km s}^{-1}$) probed by current cosmological simulations. For completeness, we transform the irregular population using the $l - v$ relation recently derived from a sample of 70 dwarf irregulars (Hoffman et al. 1996). This relation has the same form as the spiral TF relation, as well as a similar slope (6.50 ± 0.63 for the irregulars as compared to 6.76 ± 0.63 for the TF relation of Yasuda, Fukugita, & Okamura 1997).

3.3. Passband Effects

A complication in combining the published TF and FJ relations with survey luminosity functions is that slightly different filters have been used by different authors. For example, the Yasuda et al. (1997) TF relation was obtained in B_T , while the APM and UKST surveys use b_J . Table 3 gives the passband transformations (and references) used to transform the data onto comparable photometric systems. Of particular note is the R -band data. The LCRS survey data was obtained in r_g , but calibrated to the R_C system. Further, the TF data of Courteau was obtained using a Spinrad r filter, but calibrated to the r_g system. The color transformation given in Table 3 to synthesize these two data sets is derived from the transformations given by Djorgovski (1985), utilizing the galaxy color information of Fukugita, Shimasaku, & Ichikawa (1997). Correction for the effect of different passbands has a noticeable effect upon the results (e.g., v_* increases by $\sim 20 \text{ km s}^{-1}$ for SSRS2), and so must not be ignored.

3.4. Internal Extinction

A bias that is normally ignored in creation of luminosity functions is dimming due to internal absorption. While absorption is presumably negligible in ellipticals, internal absorption is significant in spirals and is a function of both inclination and luminosity (Giovanelli et al. 1995, Tully et al. 1998). Luminosity functions are inherently averaged over inclination and contain galaxies spanning a wide range of luminosity, whereas TF relations are generally calibrated with bright spirals for which the magnitudes are corrected to face-on. Consequently, it is necessary to correct the luminosity function for internal absorption before using the TF relation to transform luminosity to velocity.

The issue of internal extinction in spirals has been a source of significant debate since Valentijn’s (1990) claim that spiral galaxies are optically thick. This work was later challenged by Burstein et al. (1991) and Davies et al. (1993), who argued that Valentijn’s study was subject to significant selection effects and biases.¹ Subsequently, there has been mounting evidence, if not a consensus,

¹For a nice discussion of this topic, see Bottinelli et al. (1995).

that extinction is significant, but not as extreme as suggested by Valentijn (Giovanelli et al. 1995, Bottinelli et al. 1995, Courteau 1996, Tully et al. 1998). For this work, we adopt the extinction corrections of Tully et al. (1998, hereafter T98). Our motivation is threefold. First, and most importantly from a practical perspective, only T98 have published extinction corrections in B , R , and K — the three bands for which luminosity functions are available. Second, this is the only work other than Giovanelli et al. (1995, hereafter G95) that models dependence of absorption on luminosity.² Third, unlike Botinelli et al. (1995, hereafter B95) and G95, who concentrate on late types (Sc-Sd), the Tully sample probes a broader range of spirals. In the I -band, a comparison of T98 and G95’s results shows consistent trends, but greater extinction in G95, possibly due to the sample composition (Tully et al. 1998). Similarly, B95’s average extinction is higher than for T98. A comparison of the effects of using B95 and T98 is shown in Figure 1(a) (see §4). While the correspondence is good, we caution that this topic remains far from settled, and the extinction correction is one of the most significant sources of uncertainty in constructing $\Psi(\log v)$.

When averaged over inclination, assuming randomly distributed inclination angles,³ the luminosity corrections derived from T98 are:

$$M_{B_J}^{cor} = \frac{1}{0.92} [M_{B_J} + 0.08(15.6 + 5 \log h_{80})], \quad M_{B_J} < -15.6 \quad (7)$$

$$M_{R_C}^{cor} = \frac{1}{0.95} [M_{R_C} + 0.05(16.2 + 5 \log h_{80})], \quad M_{R_C} < -16.2 \quad (8)$$

$$M_{K'}^{cor} = \frac{1}{0.99} [M_{K'} + 0.01(18.3 + 5 \log h_{80})], \quad M_{K'} < -18.3 \quad (9)$$

The formalism for inclusion of this luminosity dependent extinction correction within the generalized Schechter function is given in the Appendix.⁴

4. Analysis and Results

²Such a dependence is expected, and is closely linked to the morphological type dependence given in the Third Reference Catalogue (de Vaucouleurs et al. 1991).

³We assume, as in Tully et al. (1998), that the aspect ratio of an edge-on spiral is $b/a = 0.2$

⁴This is in fact a simplification. The observed luminosity function is a convolution of the face-on luminosity function with an extinction-induced, asymmetric magnitude dispersion function. To account for extinction correctly, it is necessary to deconvolve the luminosity function to face-on. This would slightly flatten the faint end slope, but the effect is significantly smaller than other sources of error, so we simply note the existence of this generally overlooked effect. Also, we note that intrinsic scatter in the TF and FJ relations lead to a similar effect.

4.1. SSRS2

With all the ingredients assembled, we now construct a velocity function from the SSRS2 luminosity function. A first test is to assess the impact of internal extinction in the spiral population. Figure 1(a) shows the extinction-corrected and uncorrected spiral velocity functions, $\Psi(\log v_c)$. To illustrate the impact of the choice of extinction correction, both the T98 and B95 extinction laws are applied. The net effect of both corrections is to shift the function to higher velocity by approximately 30 km s^{-1} . The Tully correction is utilized in all subsequent figures. Next, the impact of different choices for TF and FJ relations is assessed. Figure 1(b) shows that the relations published by Yasuda et al. (1997) and Richter et al. (1987) are consistent, whereas the disparate values for the FJ relation lead to a significant change at high velocities. For the “Best” relation, spirals provide the greatest contribution at all velocities; for the “High” relation, ellipticals dominate above v_* . This is driven by the change in zeropoint.

The total velocity function can be seen as the heavy solid curve in Figure 1(c), with the two light solid lines tracing the central curve indicating the uncertainty due to the formal (1σ) statistical errors from the luminosity function and TF parameters. Also displayed are the constituent velocity functions for each morphological type, using the Yasuda, Fukugita, and Okamura (1997), deVaucouleur and Olson (1982), and Hoffman et al. (1996) $l-v$ relations for spirals, ellipticals/S0’s, and irregulars, respectively. Readily apparent is the dominance of the spiral population. Only at velocities well above v_* does the elliptical population contribute substantially. Given this dominance, it is of interest to ask how the total velocity function would differ under the assumption that all galaxies are spirals. Namely, how important is the segregation between morphological types in the translation of luminosity to velocity? From Figure 1(d) it can be seen that this “spiral approximation” is quite good, altering the total velocity function (Composite #1) by $\sim 10\%$, less than the formal errors. The validity of such an approximation is important if we wish to compare with LF surveys that lack morphological information.

There are several important notes of caution which should be mentioned. If the zeropoints of the $l-v$ relations are significantly in error, then at high velocities the elliptical population may dominate. To assess the magnitude of this effect, we plot Composite #2 in Figure 1(d), which uses the “High” FJ relation. Composite #2 has an $\sim 20\%$ higher amplitude than the spiral approximation near v_* , and has a steeper slope above v_* . Also, demonstration that the spiral population is dominant in the B -band SSRS2 does not assure that the same is true for galaxy samples selected in other bands, as we may be observing substantially different galaxies (Loveday 1998). For R -band and bluer bands, this should be a mild effect. In comparison to B -band, ellipticals in the R -band are ~ 0.15 mag brighter relative to spirals (Fukugita, Shimasaku, & Ichikawa 1997). By K -band however, the spiral approximation should be very poor. As compared to B -band, ellipticals in K are $\gtrsim 1$ mag brighter relative to spirals. Consequently, use of the spiral approximation will artificially inflate both the derived v_* and Ψ_* . In the next section we compare velocity functions derived from different surveys in order to provide a lower limit for the systematic errors that are no doubt present. For completeness we include a K -band survey, which illustrates the breakdown

of the spiral approximation.

4.2. Survey Comparison

SSRS2 is the only survey for which it is possible to generate velocity functions for each morphological type, and so it is necessary to employ the spiral approximation if we wish to compare velocity functions from different surveys. This is done for the SSRS2, APM, UKST/Durham, and LCRS (Marzke et al. 1998, Loveday et al. 1992, Ratcliffe 1998, Bromley et al. 1998), and also for a K -band survey by Gardner et al. 1997. For the B -band surveys, the TF relation of Yasuda, Fukugita, & Okamura (1997) is utilized. For the R - and K -bands we use the work of Courteau (1997) and Malhotra et al. (1996), respectively. The values of the parameters in each of these relations are given in Table 2. The resulting $\Psi(\log v_c)$ are displayed in Figure 2; Figure 3 shows the same data, but only in the regime where the TF relation is also constrained. The generalized Schechter parameters (Eq. 2) corresponding to these velocity functions are given in Table 4.

The R - and B -band data all agree within the quoted observational errors. This can be seen by comparing the parameter values in Table 4. We also illustrate this in Figure 4 by plotting $\Psi_{240} = \Psi(\log v_c)$ at $v_c = 240 \text{ km s}^{-1}$ for each survey. One important note is that, for the LCRS catalog, Figure 2 is more indicative of the actual agreement in β than is the value in Table 4. This is because the fit in Figure 2 is the sum of Schechter functions used to fit individual spectroscopic clans, whereas the value in Table 4 is derived using a single Schechter fit which is a visibly bad match to the data at the faint end (Lin et al. 1996, Bromley et al. 1998). We also note that a rough conversion of the CfA survey data to the B -band is possible via the transformation $M_{B_T} = M_Z - 0.45$ (Shanks et al. 1984). We do not plot the CfA velocity function in Figure 2, but find that it is consistent with the B - and R -band velocity functions.

The K -band data primarily serves to emphasize the limitations of this approach. For K , both v_* and Ψ_* are high relative to the other surveys. The quoted errors are large, but the difference in the resulting velocity function is statistically significant. This is not surprising, as there are several reasons to expect the K -band velocity function to be discrepant. First, and most importantly, the spiral approximation *should* break down in K , as discussed at the end of §4.1. Consequently, for future K -band surveys morphological information will be necessary if they are to be used to generate a velocity function. In addition, the Gardner et al. (1998) K -band luminosity function assumes a value of $q_0 = 0.02$. Recent supernovae surveys indicate that a more likely value is $q_0 \approx -0.5$ for a flat universe (Perlmutter et al. 1998), and so there is an additional uncertainty that we have not included in the error budget, which may decrease Ψ_* and increase v_* by $\sim 20\%$.

Furthermore, of the three bands used, the TF relation is least well-established in the K -band. Three notable recent determinations of the K -band TF relation are provided by Malhotra et al. (1996), Tully et al. (1998), and de Grijs & Peletier (1999). The parameters for each are given in Table 2. Consistent slopes are found by all three groups, but the zeropoint variation is large. The

zeropoint from T98 is dependent upon the assumed distance to Ursa Major (Verheijen 1997), and also no errors are quoted. de Grijs & Peletier quote a $1\text{-}\sigma$ error of 1.58 magnitudes. Malhotra et al., whose TF relation we employ, have the smallest quoted errors, but their TF relation is based on DIRBE observations of only 7 Local Group galaxies including the Milky Way.

4.3. Comparison with Simulations

Although the comparison of the velocity function with a halo velocity function derived from N-body simulations is more straightforward than a corresponding luminosity function comparison, there are a few caveats. The first of these concerns how to assign an appropriate value of v_c to each simulated dark matter halo, and the second concerns the association of very high- and low-velocity halos with galaxies.

It has been known for some time that the density profiles of simulated dark matter halos are not well-approximated by isothermal spheres (see e.g., Navarro, Frenk, & White 1996 and references therein). Unlike isothermal spheres, which have flat circular velocity curves, the maximum rotation velocities of halos are not the same as their virial velocities. Galaxy formation also affects dark matter halo velocity curves due to the infall of cool baryons. There are thus at least three possibilities for the v_c to use in constructing a halo velocity function:

1. $v_c = v_{\text{vir}} \equiv \sqrt{GM_{\text{vir}}/R_{\text{vir}}}$, the circular velocity of the halo at its virial radius, R_{vir} .
2. $v_c = v_{\text{max}}$, the maximum rotation velocity of the halo.
3. $v_c = v_{\text{max}}^{\text{corr}}$, the maximum velocity of the halo after baryonic infall has occurred.

Clearly, option 1 is inappropriate. Recall that v_c is the circular velocity measured at the flat part of a disk galaxy rotation curve. Halo velocity curves typically flatten at 10 – 20% of the virial radius, and v_{vir} may be as small as 60% of v_{max} (Bullock et al. 1999a). So, although halo v_{vir} velocity functions are the most straightforward of the three to estimate, we will not do so here in order to focus on the more appropriate options. Choice 2 is more sensible, and only slightly more complex to estimate, as long as density profile information is known about the dark matter halos under consideration. Option 3, correcting the halo velocity curve for the effects of baryonic infall, is, in principle, even more appropriate. However, the uncertainties associated with this correction are large. In the discussion that follows, we will explore both options 2 and 3, making use of very high-resolution simulation output that supplies the accurate spatial information needed for such an analysis.

The Adaptive Refinement Tree (ART) N-body code (Kravtsov, Klypin, & Khokhlov 1997) reaches high force resolution by refining the grid in all high-density regions. It allows the identification of distinct virialized halos as well as halos that exist as substructure within larger halos. Klypin et al. 1999b have used the combined results from two Λ CDM ($\Omega_0 = 1 - \Omega_\Lambda = 0.3$, $h = 0.7$,

$\sigma_8 = 1.0$) ART simulations to explore the velocity function of halos over a wide range of halo circular velocities (defining $v_c = v_{\text{max}}$.) The first simulation uses a $60h^{-1}\text{Mpc}$ box with a particle mass of $m_p = 1.1 \times 10^9 h^{-1} M_\odot$ and the second simulation uses a $7.5h^{-1}\text{Mpc}$ box with $m_p = 1.7 \times 10^7 h^{-1} M_\odot$. They find that the halo circular velocity function over the range $v_c \simeq 20 - 400 \text{ km s}^{-1}$ is well-described by a power law: $\Psi_{\text{halo}}(\log v_c) \simeq 0.2 \times 10^{-2.75\eta_{100}}$, where $\eta_{100} = \log(v_c/100 \text{ km s}^{-1})$. This form of $\Psi_{\text{halo}}(\log v_c)$ is shown by the thin solid line in Figure 2. We see that near v_* , the observations are in reasonable agreement with the simulations, although the density of simulated halos is slightly low. Correcting this relation for baryonic infall will help to alleviate this discrepancy, as we discuss below.

For $v_c \sim 400 \text{ km s}^{-1}$, the slope of $\Psi_{\text{halo}}(\log v_c)$ is shallower than that observed. This is not of great concern however, since high-velocity halos correspond to groups and clusters of galaxies and should not be compared directly with the observed galaxy velocity functions. Modeling galaxies in clusters is a difficult problem and is beyond the scope of this paper. However, as a first step in identifying the appropriate halos for the galaxy velocity function comparison, we can restrict ourselves to halos which are “simple” in the sense that they contain no significant substructure. Using the $60h^{-1}\text{Mpc}$ ART simulation and methods outlined in Bullock et al. (1999a), we identify halos with significant substructure as those containing at least one subhalo with $v_c \gtrsim 120 \text{ km s}^{-1}$ within the virial radius.⁵ Our simple-halo velocity function is shown by the filled circles connected by the dashed line in Figure 2. The errors on these points reflect Poisson uncertainties. This first-order correction to the pure halo velocity function demonstrates a similar fall-off as that observed; however, the slope remains too shallow for $v_c \gtrsim 400 \text{ km s}^{-1}$. It is likely that if the substructure criteria for simple halos was more stringent, for example, if we exclude all halos with substructure with $v_c \gtrsim 70 \text{ km s}^{-1}$, then the simple halo velocity function might more closely mirror the data at high v_c . Higher-resolution simulations would be needed to check this.

Below about 120 km s^{-1} the halo number density exceeds the galaxy number density. There are several factors which may contribute to this excess. It is possible that some fraction of lowest-velocity halos are not associated with galaxies, as the baryonic material may be ionized and unable to cool and form galaxies (Efstathiou 1992, Weinberg, Hernquist, & Katz 1997). Another factor may be selection effects in luminosity function surveys, in the sense that low surface brightness galaxies are systematically missed (Sprayberry et al. 1997, Dalcanton 1998). An example of this is LCRS, for which a surface brightness limit was imposed upon the spectroscopic sample used to construct the LF (Shectman et al. 1996). Inclusion of these galaxies can act to steepen the faint end slope of the observed luminosity function, and hence the observed velocity function. One intriguing observation is that the orbits of satellite galaxies exhibit polar anisotropy (Zaritsky et al. 1997), and the suggestion that this may result from the destruction or inhibited formation of a large population of satellites near the plane of the disk of spiral galaxies (Zaritsky & Gonzalez

⁵We are unable to push this criterion to a lower value of v_c due to the incompleteness of our halo catalog, reflecting the finite resolution of the simulation.

1999). Such a scenario could help resolve the discrepancy, but currently there exists no known physical process that could accomplish such destruction or inhibition.

Although a direct comparison with the halo velocity function is an interesting first step, for a detailed comparison one must correct the results of the dissipationless halo v_c for the effect of baryonic infall. As a galaxy forms at the center of a halo, the maximum rotation velocity of the system increases both due to direct gravitational effects of the disk and the contraction that infall induces on the halo. The overall shift in the velocity function will depend on the nature of the infall and the processes of disk formation; these are in principle functions of the initial halo v_c and how the galaxy was assembled including cooling and supernovae feedback.

Assuming that the infall of gas is adiabatic and that gas infall is halted due to angular momentum support of the disk (Fall & Efstathiou 1980), Blumenthal et al. (1986) describes a convenient analytic model for calculating the rotation curve redistribution during the process of disk formation (see also Flores et al. 1993 and Dalcanton, Spergel & Summers 1997). Mo, Mao, & White (1997) provide a useful fitting function for the infall-corrected maximum rotation velocity of dark matter halos:

$$v_c \simeq v_c^{\text{halo}} \left[1 + 4.34m_d - 3.76m_d^2 \right] F_V(c_{\text{vir}}, \lambda, m_d), \quad (10)$$

where v_c^{halo} is the maximum rotation velocity of the halo before infall and

$$F_V(c_{\text{vir}}, \lambda, m_d) = 2.15 \left(\frac{\lambda}{0.1} \right)^{-2.67m_d - 0.0038/\lambda + 0.2\lambda} \left[1 + \frac{c_{\text{vir}}}{17.5} - \left(\frac{c_{\text{vir}}}{54} \right)^2 - \frac{1.54}{c_{\text{vir}}} \right] c_{\text{vir}}^{-1/2}. \quad (11)$$

Here, m_d is the fraction of the total halo mass that forms the disk, $\lambda \equiv J|E|^{1/2}G^{-1}M^{-5/2}$ is the dimensionless angular momentum parameter (where J and E are the total angular momentum and energy of the halo), and $c_{\text{vir}} = R_{\text{vir}}/R_s$ describes the nature the dark matter halo density profile, which is assumed to be of the Navarro, Frenk, & White (1996) form: ⁶ $\rho_{\text{NFW}}(r) = \rho_s[(r/R_s)(1 + r/R_s)^2]^{-1}$. (The normalization parameter, ρ_s , is determined by v_c^{halo} if R_s and c_{vir} are given.) We have implicitly assumed that the fraction of the total halo angular momentum in the disk is equal to the fraction of mass in the disk, $j_d = m_d$. Using Equation 10, we may correct the velocity function obtained from the simulations by using appropriate values for λ , c_{vir} , and m_d . This may be done halo by halo, but for simplicity we use the respective averages of these quantities as a function of v_c^{halo} .

By analyzing the $60h^{-1}\text{Mpc}$ ART simulation, Bullock et al. (1999a) find that the average halo concentration obeys

$$c_{\text{vir}}(v_c^{\text{halo}}) \simeq 13 \sqrt{\frac{v_c^{\text{halo}}}{200 \text{ km s}^{-1}}} \quad (12)$$

⁶Although there is disagreement (cf. Kravtsov et al. 1998, Primack et al. 1998, Moore et al. 1999) about the detailed shape of dark matter halo profiles at very small radii, $r \lesssim 0.02$, these very inner regions are not important for determining v_{max} , so the NFW profile is appropriate for our needs.

and the average spin parameter is roughly constant as a function of the halo circular velocity $\langle \lambda \rangle \simeq 0.04$ (Bullock et al. 1999b). The main uncertainty in this calculation is m_d , the fraction of halo mass that ends up the disk. This quantity depends on the details of galaxy formation, including gas cooling and supernovae reheating. Due to the complexity of the problem, we have used the (fiducial) semi-analytic models (SAMs) of galaxy formation developed by Somerville & Primack (1999) in order to determine a reasonable form for $m_d(v_c^{\text{halo}})$. Using the Λ CDM cosmology described above, we find that the following fitting function

$$m_d(x) \simeq 0.1 \frac{x - 0.25}{1 + x^2}, \quad (13)$$

where $x \equiv v_c^{\text{halo}}/(200 \text{ km s}^{-1})$, does well in reproducing the average m_d of SAM galaxies over the range of velocities $v_c \simeq 60 - 350 \text{ km s}^{-1}$. These models assume $\Omega_b = 0.020h^{-2}$ (Burles & Tytler 1998). Note that m_d rises with v_c for $v_c^{\text{halo}} \lesssim 200 \text{ km s}^{-1}$; this is a result of supernova explosions, which act to remove gas more effectively from smaller galaxies, as proposed in Dekel & Silk (1986). After reaching a maximum of ~ 0.04 near $v_c^{\text{halo}} \sim 200 \text{ km s}^{-1}$, the value of m_d slowly declines because a smaller fraction of gas in large halos has time to cool.

Using Equations 10-13 we have corrected the halo velocity function for the effect of infall. This correction, which we will refer to as the SAM infall model, is shown by the heavy solid curve in Figures 2 and 3. The curvature in the SAM infall model is caused by the varying behavior of m_d (Eq. 13). For reference, the medium weight line shows the result of the infall correction when the mass fraction of the disk is held constant at $m_d = 0.04$. The flattening of the SAM-corrected curve at small velocities is due to the inability of small disks to retain their gas — as the disk mass becomes smaller relative to the mass of the halo, the correction to the halo circular velocity becomes negligible. The bend in the SAM-corrected velocity curve at large v_c is because not all of the gas in large halos has time to cool. The SAM infall is truncated at $v_c \gtrsim 350 \text{ km s}^{-1}$ because the infall calculation is inappropriate for group- and cluster-mass halos. We also truncate the curve below $v_c = 100 \text{ km s}^{-1}$, where $m_d \lesssim 0.02$. Below this value the infall-correction formula (10) ceases to be a good fit (Mo, Mao, & White 1998); however, it is likely that galaxies with any smaller amount of gas will be of very low surface brightness and difficult to detect.

It is obvious from this comparison that the halo velocity function differs markedly from the galaxy velocity function, but there are avenues of theoretical exploration which may help in understanding the differences. At velocities well above v_* , most halos correspond to groups and clusters rather than individual galaxies. Understanding the fall-off of the velocity function at high v_c will require more detailed modeling of galaxy formation within clusters, perhaps using both semi-analytic and N-body techniques. Near v_* , for the Λ CDM cosmology we explore, the halo number density and slope is comparable with the galaxy density to within observational errors — see Figure 4. The halo density is slightly low without infall correction, and slightly high with the approximate infall correction we present. Below v_* the halo density exceeds the galaxy density, but the tendency for small v_c objects to have small disk mass fractions due to supernova feedback may help explain the discrepancy: because they have low luminosity and low surface brightness, many low- v_c

galaxies will be missed in the luminosity functions we started from. If, however, the discrepancy at the low- v_c end is not purely due to selection effects, it may turn out to pose a real challenge for theory. More detailed modeling of redshift survey selection effects and of small-velocity galaxies, including consistent treatments of gas cooling, baryonic infall, supernova feedback, and disk surface brightnesses will be needed to explore this problem in detail.

5. Discussion and Conclusions

A main goal of this work was to evaluate the robustness with which $\Psi(\log v_c)$ can currently be estimated. While morphological information was incorporated in converting the SSRS2 luminosity function to a velocity function, a key result of this detailed analysis is that treating the entire population as spirals does not significantly alter the resulting velocity function.⁷ Furthermore, while the normalization of the velocity function remains poorly constrained ($\sim 30\%$ variance in Ψ_* among surveys (excluding K), and a factor of 2 variance in $\Psi(\log v_c)$ at $v_c = 240 \text{ km s}^{-1}$), the *shape* of the velocity function is similar for all input luminosity functions. Both the shape and normalization are also consistent within the errors with the velocity function derived by Shimasaku (1993).

The key benefit of our approach is that the models needed to connect N-body simulations and observations become much less complex when we use observed TF relations and extinction corrections instead of trying to reproduce these functions via the semi-analytic models. This contrasts with SAMs, which output modelled $l-v$ relations that are dependent on tunable model parameters (e.g., star formation timescales, supernovae feedback, etc.) for comparison with observations. Another benefit is that, by converting to velocity, we provide a single target function for the models to attempt to reproduce — in contrast with luminosity functions in different bands from various redshift surveys. Hopefully, this will be of value in simplifying comparison with simulations from different groups.

The main sources of uncertainty limiting the precision with which the velocity function can be constructed via this approach are:

1. Large scatter in the reported values of Φ_* , possibly due to local deviation from mean density.
2. Selection bias at the faint end of the luminosity function, which may act to flatten the faint end slope.
3. The limited velocity range over which the TF relation is well-calibrated.

⁷Unless there is a large error in the FJ zeropoint, in which case it may be necessary to treat E's separately in order to accurately reproduce the high velocity end.

4. Uncertainty in the TF relation. Beyond the statistical errors, there are indications of several potentially significant biases in current relations. In particular, Willick and Courteau (private communication) find that using the circular velocity at two disk scale lengths (as determined by disk+bulge fitting) reduces scatter in the TF relation and also can significantly alter the slope relative to other methods of determining v_c .
5. Uncertainty regarding the extinction correction, and also over-simplified treatment of extinction by averaging over inclination.
6. Uncertainty in the zeropoint of the FJ relation. A change in the zeropoint could noticeably alter the velocity function above v_* .
7. Lack of a detailed understanding of the correspondence between σ in ellipticals and v_c in spirals. While $v_c = \sqrt{2}\sigma$ may be true on average for bright ellipticals, scatter in this relation can also alter the velocity function above v_* .
8. Intrinsic scatter in the TF and FJ relations.

Use of next-generation surveys such as Anglo-Australian 2-degree Field (2dF) and the Sloan Digital Sky Survey (SDSS) will reduce the cosmic variance of Φ_* . Further, an alternative approach to this technique would be the direct construction of the velocity function from a galaxy survey designed to obtain both photometry and slit-based spectral linewidths. This could be achieved by a slitmask survey of a volume-limited subset of the SDSS or 2dF samples.⁸ Bypassing the $l - v$ relations would significantly reduce uncertainty in the derived velocity function, although it would be necessary to separate the spiral and elliptical populations so as to treat rotationally- and thermally-supported systems correctly. Finally, with the multi-color photometry of SDSS, it will be possible to measure inclinations and correct for extinction effects on a galaxy-by-galaxy basis prior to construction of the luminosity function.

In the meantime, we have demonstrated that existing data is sufficient to construct the velocity function accurate to within roughly a factor of two at a given velocity, which is suitably accurate for comparison with predictions from cosmological N-body simulations. By comparison with one such Λ CDM simulation, we have illustrated the usefulness of this approach. The main sources of uncertainty limiting the precision with which the velocity function can be estimated theoretically are:

1. The degree to which halos with very large and very small v_c should be associated with galaxies.
2. Uncertainties associated with correcting the v_c of measured halos for the effect of baryonic infall.

⁸While 2dF and SDSS both obtain spectral information, the fiber-fed spectrographs only collect information on galactic centers, and hence do not provide information on the rotation curves of spiral galaxies.

There is reasonable agreement between the observations and simulations near v_* , and the exploration of these uncertainties may help explain the large excess of systems in the simulations below $\sim 120 \text{ km s}^{-1}$ and the slope of the velocity function above v_* . This poses an interesting challenge for models of galaxy formation to address. A key test will be to see if the incorporation of baryonic infall and cooling physics leads to a theoretical galaxy velocity function consistent with those observed.

6. Acknowledgements

The authors would like to thank the anonymous referee for suggestions which significantly improved this paper, especially regarding the need to include passband corrections. We also thank Dennis Zaritsky, Raja Guhathakurta, Sandra Faber, Stephane Courteau, Jeff Willick, and Chris Kochanek for helpful discussions regarding this research. AHG and KAW acknowledge support from the NSF Graduate Research Fellowship Program. JSB, TSK, and JRP were supported by a NASA ATP grant.

A. Appendix

Starting with the Schechter function,

$$\Phi(L)dL = \Phi_* \left(\frac{L}{L_*}\right)^\alpha \exp\left(-\frac{L}{L_*}\right) d\left(\frac{L}{L_*}\right), \quad (\text{A1})$$

and the relation

$$L = Ax^n, \quad (\text{A2})$$

where A is a constant, we define

$$\tilde{\Psi}(x)dx = \Phi(L)dL \quad (\text{A3})$$

$$= \Phi_* \left(\frac{x}{x_*}\right)^{n\alpha} \exp\left[-\left(\frac{x}{x_*}\right)^n\right] n \left(\frac{x}{x_*}\right)^{n-1} d\left(\frac{x}{x_*}\right). \quad (\text{A4})$$

$$= n\Phi_* \left(\frac{x}{x_*}\right)^{n\alpha+n-1} \exp\left[-\left(\frac{x}{x_*}\right)^n\right] d\left(\frac{x}{x_*}\right). \quad (\text{A5})$$

Thus,

$$\tilde{\Psi}(x)dx = \tilde{\Psi}_* \left(\frac{x}{x_*}\right)^\beta \exp\left[-\left(\frac{x}{x_*}\right)^n\right] d\left(\frac{x}{x_*}\right), \quad (\text{A6})$$

where $\beta \equiv n(\alpha + 1) - 1$ and $\tilde{\Psi}_* \equiv n\Phi_*$.

Inclusion of a magnitude dependent extinction correction of the form,

$$M^{cor} = \gamma^{-1}(M + C), \quad (\text{A7})$$

where γ and C are constants, is equivalent to modifying the power and zeropoint of the $L-x$ relation. Specifically, for the case of a TF relation (which in general will be extinction corrected) of the form,

$$M^{cor} = a - b(\log 2v_c - 2.5), \quad (\text{A8})$$

in order to relate v to the observed magnitude, M , from a luminosity function survey (which in general will *not* be extinction corrected), we substitute

$$M^{cor} = \gamma^{-1}(M + C) = a - b(\log 2v_c - 2.5), \quad (\text{A9})$$

or,

$$M = (\gamma a - C) - \gamma b(\log 2v_c - 2.5) = a' - b'(\log(\Delta v) - 2.5). \quad (\text{A10})$$

The resulting modified TF relation is thus of the same form as the original, but with a new slope and offset that are related to the old ones by

$$a' = \gamma a - C, \quad (\text{A11})$$

and

$$b' = \gamma b. \quad (\text{A12})$$

REFERENCES

- Alonso, M.V., da Costa, L.N., Pellegrini, P.S., & Kurtz, M.J. 1993, AJ, 106, 676
- Binney, J., & Tremaine, S. 1987, *Galactic Dynamics* (Princeton University Press, Princeton), p. 230
- Bottinelli, L., Gouguenheim, L., Paturel, G., & Teerikorpi, P. 1995, A&A, 296, 64
- Bromley, B.C., Press, W.H., Lin, H., & Kirschner, R.P. 1998, ApJ, 505, 25
- Blumenthal, G.R., Faber, S.M., Flores, R., & Primack, J.R. 1986, ApJ, 301, 27
- Bullock, J.S., Kolatt, T.S., Sigad, Y., Somerville, R.S., Kravtsov, A.V., Klypin, A.A., Primack, J.R., & Dekel, A. 1999a (in preparation)
- Bullock, J.S., Kolatt, T.S., Sigad, Y., Kravtsov, A.V., Klypin, A.A., Primack, J.R., & Dekel, A., 1999b (in preparation)
- Burles, S. & Tytler, D. 1998 astro-ph/9803071
- Burstein, D., Haynes, M.P., Faber, S.M. 1991, Nature, 353, 486
- Cole, S., Aragon-Salamanca A., Frenk C., Navarro J., Zepf S., 1994, MNRAS, 271, 781
- Cole, S., Kaiser, N. 1989, MNRAS, 237, 1127

- Colin, P., Klypin, A.A., Kravtsov, A.K., & Khokhlov, A., ApJ(submitted), astro-ph/9809369
- Courteau, S. 1997, ApJS, 103, 363
- Courteau, S. 1997, AJ, 114, 2402
- Dalcanton, J.J., Spergel, D.N., Summers, F.J. 1997, ApJ, 482, 659
- Dalcanton, J.J. 1998, ApJ, 495, 251
- Davies, J.I., Phillips, S., Boyce, P.J., Disney, M.J. 1993, MNRAS, 260, 491
- de Grijs, R. & Peletier, R.F. 1999, astro-ph/9906293
- de Vaucouleurs, G., de Vaucouleurs, A., Corwin, H.G., Jr., Buta, R.J., Paturel, G., & Fouque, P. 1991, Third Reference Catalogue of Bright Galaxies (New York: Springer)
- de Vaucouleurs, G., & Olson, D.W. 1982, ApJ, 256, 346
- Dekel, A. & Silk, J. 1986, ApJ, 303, 39
- Dressler, A., Lynden-Bell, D., Burstein, D., Davies, R.L., Faber, S.M., Terlevich, R., & Wegner, G. 1987, ApJ, 313, 42
- Efstathiou, G. 1992, MNRAS, 256, 43
- Faber, S.M. & Jackson, R.E. 1976, ApJ, 204, 668
- Fall S.M. & Efsathiou G. 1980, MNRAS, 193, 189
- Flores, R., Primack, J.R., Blumenthal, G.R., & Faber, S.M. 1993, ApJ, 412, 443
- Fukugita, M., Shimasaku, K., & Ichikawa, T. 1997, PASP, 107, 945
- Gardner, J.P., Sharples, R.M., Frenk, C.S., Carrasco, B.E. 1997, ApJ, 480, 99
- Giovanelli, R., Haynes, M.P., Salzer, J.J., Wegner, G., da Costa, L.N., & Freudling, W. 1995, AJ, 110, 1059
- Hoffman, G.L., Salpeter, E.E., Farhat, B., Roos, T., Williams, H., & Helou, G. 1996, ApJS, 105, 269
- Kauffmann, G., White, S.D.M., Guiderdoni, B., 1993, MNRAS, 264, 201
- Klypin, A.A., Kravtsov, A.V., Valenzuela, O., & Prada, F. 1999, astro-ph/9901240
- Kolatt, T.S., Bullock, J.S., Somerville, R.S., Sigad, Y., Jonsson, P., Kravtsov, A.V., Klypin, A.A., Faber, S.M., Primack, J.R., & Dekel, A. 1999, ApJ, in press.
- Kravtsov, A.V., Klypin, A.A., Bullock, J.S., & Primack, J.R., 1998, ApJ, 502, 48

- Kravtsov, A.V., Klypin, A.A., Khokhlov, A.M. 1997, *ApJS*, 111, 73
- Lin, H., Kirshner, R. P., Sheckman, S. A., Landy, S. D., Oemler, A., Tucker, D. L., & Schechter, P. L. 1996, *ApJ*, 464, 60
- Loveday, J. 1998, *astro-ph/9810131*
- Loveday, J., Peterson, B.A., Efstathiou, G., Maddox, S.J. 1992, *ApJ*, 390, 338
- Malhotra, S., Spergel, D., Rhoads, J.E., & Li, J. 1996, *ApJ*, 473, 687
- Marzke, R.O., Geller, M.J., Huchra, J.P., & Corwin, H.G. 1994, *AJ*, 108, 437
- Marzke, R.O., da Costa, L.N., Pelligrini, P.S., Willmer, C.N.A., & Geller, M.J. 1998, *ApJ*, 503, 617
- Mo, H.J., Mao, S., & White, S.D.M. 1998, *MNRAS*, 295, 319
- Moore, B., Quinn, F., Governato, J., Stadel, J., Lake, G., 1999, *astro-ph/9903164*
- Navarro, J.F., Frenk, C.S., & White, S.D.M. 1996, *ApJ*, 462, 563
- Perlmutter, S. et al. 1998, *ApJ*(in press), *astro-ph/9812133*
- Primack, J.R., Bullock, J.S., Klypin, A.A., & Kravtsov, A.V., to appear in *Galaxy Dynamics*, ASP Conference Series, eds. D Merritt et al., *astro-ph/9812241*
- Ratcliffe, A., Shanks, T., Parker, Q.A., & Fong, R. 1998, *MNRAS*, 293, 197
- Richter, O., Tammann, G.A., & Huchtmeier, W.K. 1987, *A&A*, 171, 33
- Schechter, P. 1976, *ApJ*, 203, 297
- Sheckman, S.A., Landy, S.D., Oemler, A., Tucker, D.L., Lin, H., Kirshner, R.P., & Schechter, P.L. 1996, *ApJ*, 470, 172
- Shanks, T., Stevenson, P., Fong, R., & MacGillivray, H. 1984, *MNRAS*, 206, 767
- Shimasaku, K. 1993, *ApJ*, 413, 59
- Bullock, J.S., Somerville, R.S., Kravtsov, A.V., Klypin, A.A., Primack, J.R., & Dekel, A. 1999 (in preparation)
- Somerville, R.S., & Primack, J.R. 1999, *MNRAS*(in press)
- Sprayberry, D., Impey, C.D., Irwin, M.J., & Bothun, G.D. 1997, *ApJ*, 482, 104
- Tully, R.B., & Fisher, J.R.T. 1977, *A&A*, 54, 661
- Tully, R.B., Pierce, M.J., Huang, J., Saunders, W., Verheijen, M.A.W., & Witchalls, P.L. 1998, *AJ*, 115, 2264

- Valentijn, E.A. 1990, *Nature*, 346, 153
- Verheijen, M.A.W. 1997, Ph.D. thesis, Univ. Groningen
- Weinberg, D.H., Hernquist, L., & Katz, N. 1997, *ApJ*, 477, 8
- Willick, J.A., Courteau, S., Faber, S.M., Burstein, D., Dekel, A., & Kolatt, T. 1996, 457, 460
- Yasuda, N., Fukugita, M., Okamura, S. 1997, *ApJS*, 108, 417
- Zaritsky, D., Smith, R., Frenk, C., & White, S.D.M. 1997, *ApJ*, 478, L53
- Zaritsky, D. & Gonzalez, A.H. 1999, submitted to *ApJ*
- Zucca, E., Pozzetti, L., & Zamorani, G. 1994, *MNRAS*, 269, 953

Table 1. A sample of published field luminosity functions.

Survey	Band	# Galaxies	Type	M_*	α	Φ_* ($h^3 \text{ Mpc}^{-3}$)	M_{low}	M_{high}
SSRS2	B_{ssrs2}	5306	All	-19.43 ± 0.06	-1.12 ± 0.05	$12.8 \pm 2.0 \times 10^{-3}$	-21.1	-15.58
			E/S0	-19.37 ± 0.11	-1.00 ± 0.09	$4.4 \pm 0.8 \times 10^{-3}$	-21.1	-14.
			Sp	-19.43 ± 0.08	-1.11 ± 0.07	$8.0 \pm 1.4 \times 10^{-3}$	-21.1	-15.58
			Irr	-19.78 ± 0.50	-1.81 ± 0.24	$0.20 \pm 0.08 \times 10^{-3}$	-21.1	-14.
APM	b_J	1769	All	-19.50 ± 0.13	-0.97 ± 0.15	$14.0 \pm 1.7 \times 10^{-3}$	-21.25	-15.5
UKST	b_J	2500	All	-19.68 ± 0.10	-1.04 ± 0.08	$17.0 \pm 3.0 \times 10^{-3}$	-21.5	-14.5
CfA	Z	9063	All	-18.90	-1.02	$20.1 \pm 5.0 \times 10^{-3}$		
LCRS	r_g/R_C	22743	All	-20.29 ± 0.02	-0.70 ± 0.05	$19.0 \pm 1.0 \times 10^{-3}$	-22	-18.
			Clan 1	-20.29 ± 0.07	0.51 ± 0.14	$0.40 \pm 0.02 \times 10^{-3}$	-22.5	-18.
			Clan 2	-20.23 ± 0.03	-0.12 ± 0.05	$6.9 \pm 0.5 \times 10^{-3}$	-22.5	-16.5
			Clan 3	-19.89 ± 0.04	-0.31 ± 0.07	$8.5 \pm 0.1 \times 10^{-3}$	-22.5	-16.5
			Clan 4	-19.86 ± 0.05	-0.65 ± 0.08	$7.3 \pm 0.2 \times 10^{-3}$	-22	-16.5
			Clan 5	-19.95 ± 0.09	-1.23 ± 0.10	$1.9 \pm 0.6 \times 10^{-3}$	-21.5	-16.5
			Clan 6	-20.10 ± 0.16	-1.93 ± 0.13	$0.7 \pm 0.5 \times 10^{-3}$	-21	-17.
Gardner et al.	K	567	All	-23.30 ± 0.30	-1.00 ± 0.20	14.4×10^{-3}	-25	-20.5

Note. — For LCRS, the survey data was obtained using r_g , but calibrated to R_C . M_{low} and M_{high} denote the magnitude range over which the given Schechter function is a good fit to the data.

Table 2. Tully-Fisher parameters.

	Band	a	b	v_{low}	v_{high}
Yasuda et al. 1997	B_T	-18.71 ± 0.11	6.76 ± 0.63	67	276
Richter et al. 1987	B_T	-18.45 ± 0.39	7.17 ± 0.20	~ 10	~ 280
Hoffman et al. 1996 (Irr)	B_T	-18.13 ± 0.70	6.50 ± 0.63	~ 10	~ 80
Courteau 1997	r_s/r_g	-20.00 ± 0.03	6.17 ± 0.28	~ 90	~ 350
Malhotra et al. 1996	K	-21.41 ± 0.11	8.59 ± 0.67	117	273
de Grijs & Peletier 1999	K	-22.48 ± 1.58	8.09 ± 0.52	~ 90	~ 310
Tully et al. 1998	K'	-22.67	8.73	~ 50	~ 280

Note. — The listed values are coefficients to the equation $M=a-b (\log(\Delta v)-2.5)$, and have been normalized to $H_0=100 \text{ km s}^{-1}$. The value listed for Courteau 1997 corresponds to the determination using v_c at 2.2 optical scale lengths for the Courteau-Faber ‘quiet Hubble flow’ sample. The imaging for Courteau 1997 was obtained with a Spinrad r filter, r_s , but calibrated to r_g . In the last two columns v_{low} and v_{high} indicate the limits of the velocity range spanned by the data used to construct these TF relations.

Table 3. Passband Conversions.

Transformation	Reference
$B_{SSRS2} = B_T + 0.26$	Alonso et al. 1993
$b_J \approx B_T + 0.06$	Cole et al. 1994; Alonso et al. 1993
$r_{LCRS} \approx r_{Courteau} + 0.33$	Djorgovski 1985; Fukugita et al. 1995
$r_{LCRS} \approx R_C + 0.36$	Fukugita et al. 1995

Note. — The color transformations used to place $l - v$ relations, luminosity functions, and extinction corrections on the same filter system.

Table 4. Velocity Function Parameters

Survey	TF Relation	v_* (km s ⁻¹)	β	Ψ_* (Mpc ⁻³ h ³)
SSRS2	Yasuda	247 ± 7	-1.30 ± 0.13	7.3 ± 1.4 × 10 ⁻²
SSRS2	Richter	261 ± 15	-1.32 ± 0.13	7.8 ± 1.2 × 10 ⁻²
APM	Yasuda	253 ± 8	-0.93 ± 0.37	8.0 ± 1.3 × 10 ⁻²
UKST	Yasuda	271 ± 9	-1.10 ± 0.20	9.7 ± 2.0 × 10 ⁻²
LCRS	Courteau	215 ± 2	-0.30 ± 0.12	10.3 ± 0.7 × 10 ⁻²
Gardner	Malhotra	265 ± 11	-1.00 ± 0.68	11.3 ± 4.8 × 10 ⁻²

Note. — The listed values are the derived parameters for the velocity function using an assortment of surveys and Tully-Fisher relations. For LCRS, the published single Schechter function fit is used (Lin et al. 1996), whereas in Figure 2 the fits to the individual clans are used. Also, no error is given for Φ_* in the Gardner survey; *the error given here is an estimate based upon the relative number of galaxies in the Gardner sample compared to other surveys.* Even with no error in Φ_* however, the error in Ψ_* resulting from statistical uncertainty in the K -band TF relation would be 8.7×10^{-3} Mpc⁻³h³. Note that Ψ_* corresponds to the $(\log v_c)$ velocity function, $\Psi(\log v_c)$, the related quantity for $\tilde{\Psi}(v_c)$ is $\tilde{\Psi}_* = \Psi_*/\ln(10)$ (see Eq. 3).

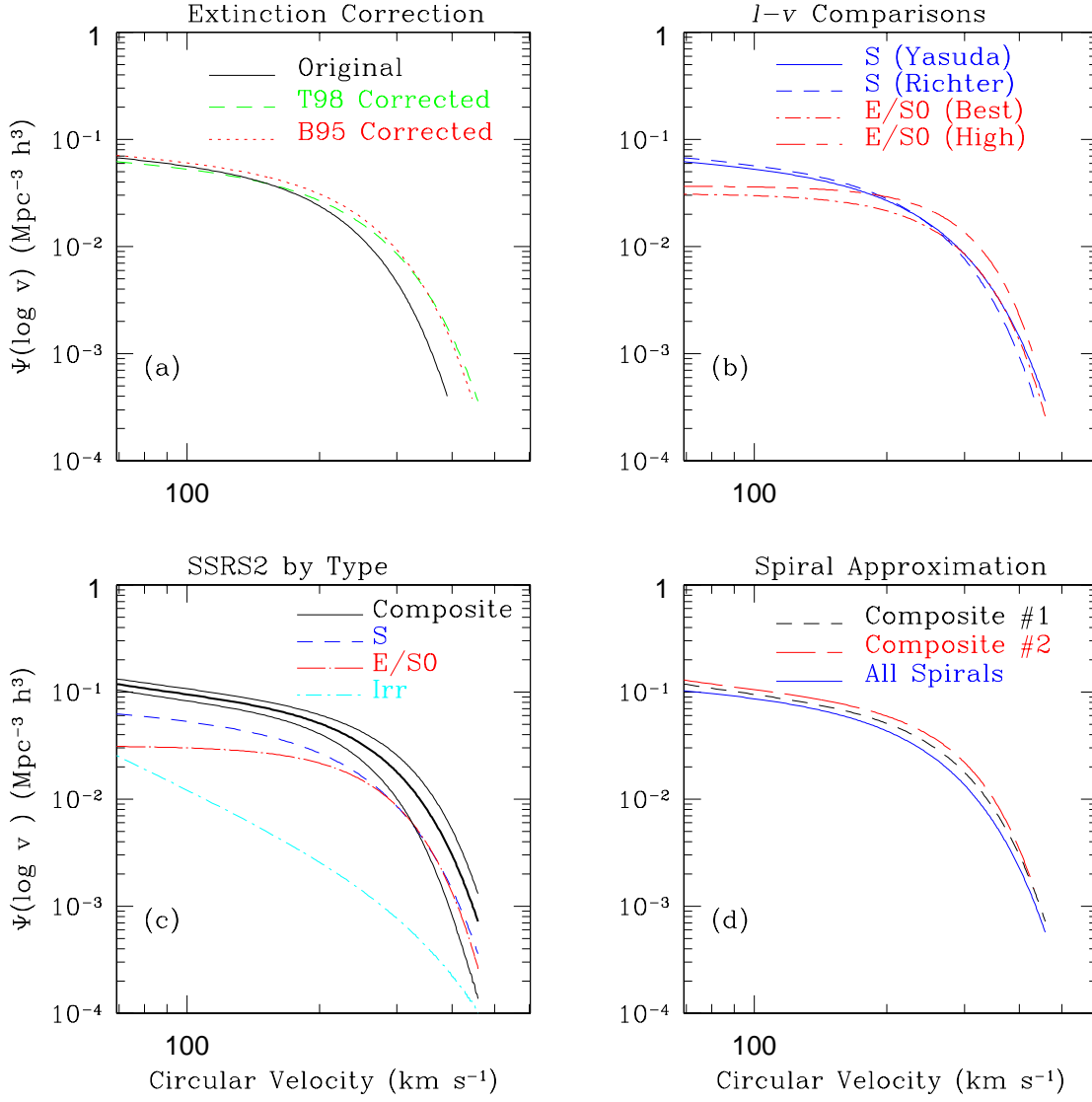


Fig. 1.— Various SSRS2 velocity function estimates: (a) Effect on spiral velocity function of correction for internal extinction, using both T98 and B95 extinction laws. The net effect of both is to shift the velocity function up by $\sim 30 \text{ km s}^{-1}$. (b) Different choices of $l-v$ relation parameters (see text). (c) Composite velocity function and contributions by each morphological class. The Yasuda TF relation and “Best” FJ relation are used. One standard deviation errors are represented by the two thin lines. (d) Differences in the derived velocity function under the assumption that all galaxies are spirals (short dashed line). Composite #1 (solid line) is the velocity function generated using the Yasuda, Fukugita, & Okamura (1997) TF relation and the “Best” FJ relation. For Composite #2 (long dashed line), the “High” FJ relation is used instead to illustrate the effect of uncertainty in the FJ relation.

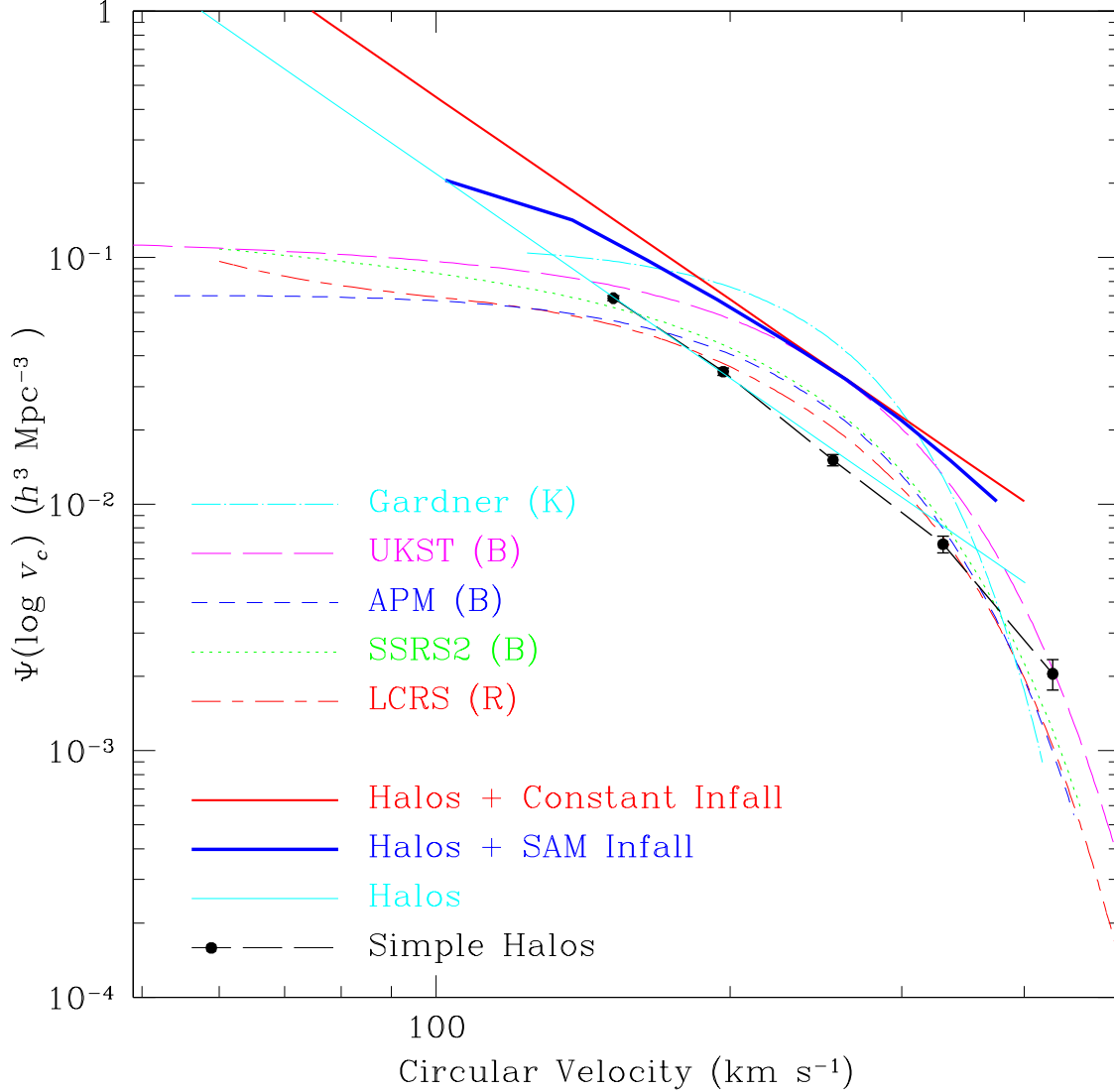


Fig. 2.— Velocity functions for five different surveys in three different bands generated using the spiral approximation. Each is plotted over the range for which a Schechter luminosity function is a good fit to the LF data. The thin solid line reflects the dark matter halo velocity functions as determined from N-body simulations. The dashed line connecting the points is the corresponding “simple halo” velocity function, which neglects all halos in the simulation with significant substructure. Also shown is the halo velocity function corrected for the effect of baryonic infall, using a constant disk mass fraction approximation (straight thin line) and a more complicated assumption based on results from semi-analytic models of galaxy formation (SAMs, bold line).

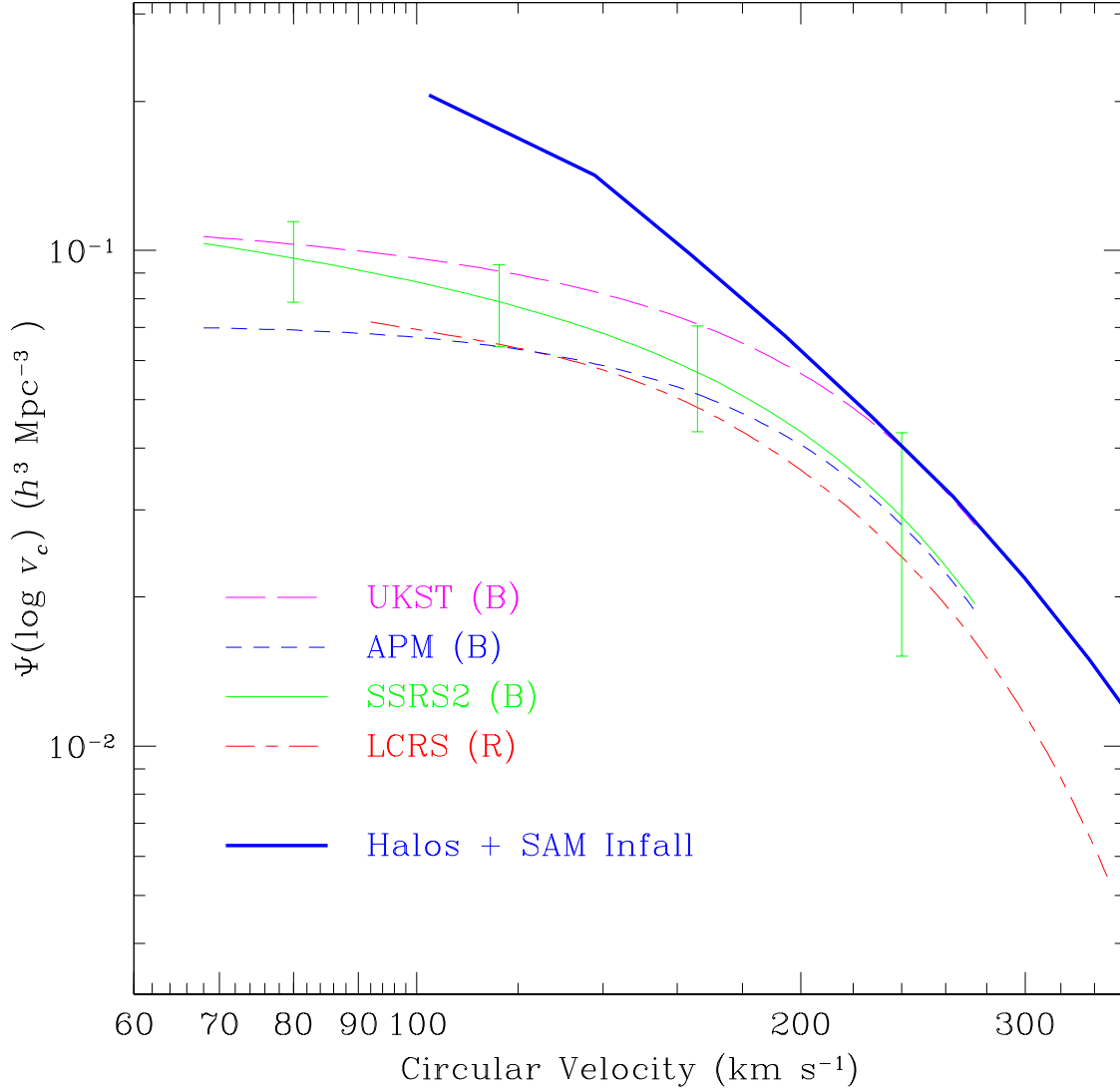


Fig. 3.— Same as Figure 2, except that the observed velocity functions are now only plotted in the region in which both the luminosity function and TF relation used to generate each velocity function are well-constrained by the data, and the K -band data is no longer plotted. For SSRS2, the line style has been changed to solid and error bars have been added. Also, for clarity only the SAM infall model is plotted.

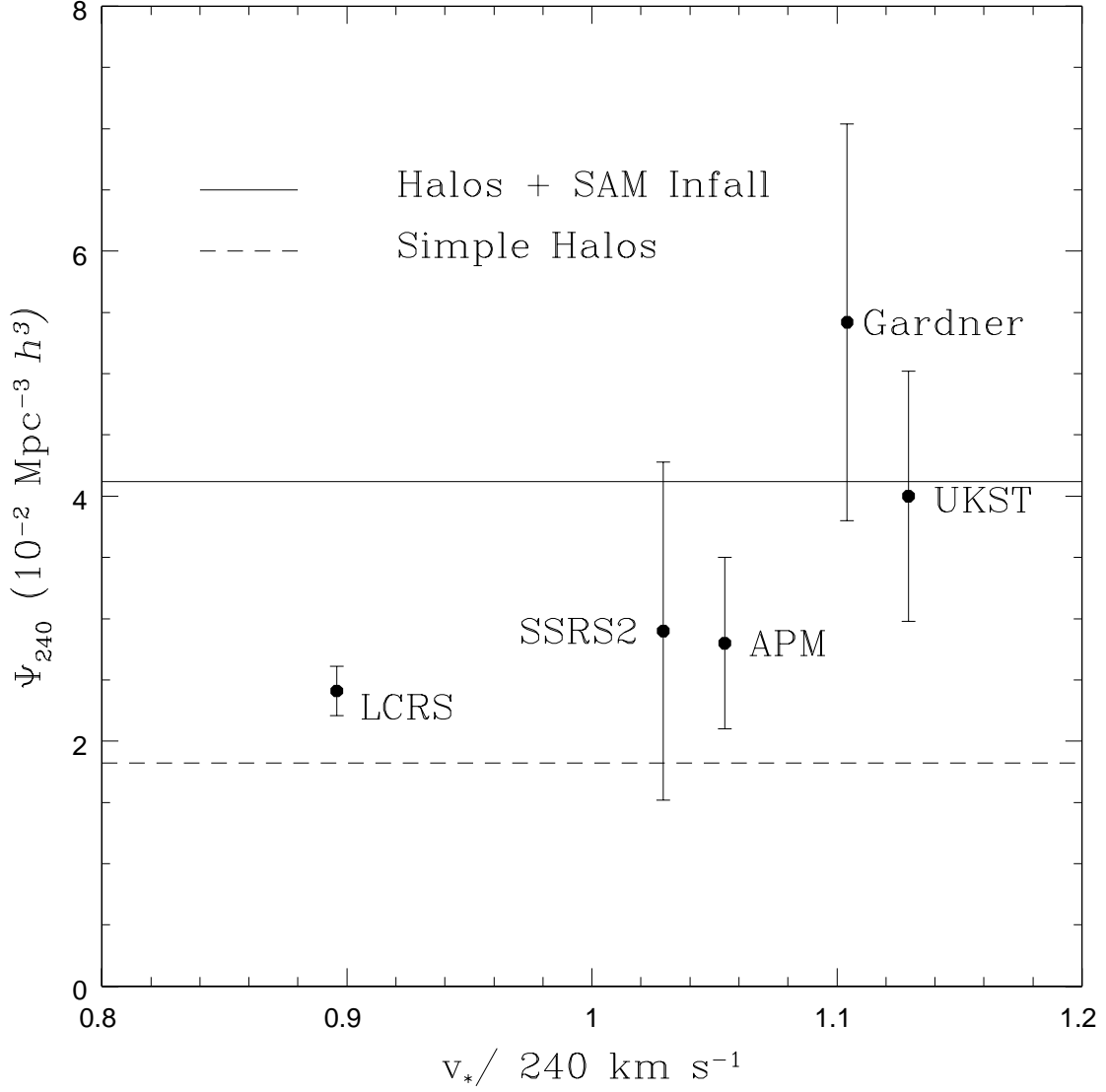


Fig. 4.— Comparison of $\Psi_{240} = \Psi(\log v_c)$ at $v_c = 240 \text{ km s}^{-1}$ for five surveys. The error bars are the formal statistical errors and do not include likely systematic effects. The x-axis is given in units of each survey’s v_* .